Absolute cross sections for electronic excitation of pyrimidine by electron impact

Khrystyna Regeta, Michael Allan, Zdeněk Mašín, and Jimena D. Gorfinkiel

---

Articles you may be interested in

Intermediate energy cross sections for electron-impact vibrational-excitation of pyrimidine
J. Chem. Phys. **143**, 094304 (2015); 10.1063/1.4929907

Absolute cross sections for vibrational excitations of cytosine by low energy electron impact
J. Chem. Phys. **137**, 115103 (2012); 10.1063/1.4752655

Absolute electronic excitation cross sections for low-energy electron (5 – 12 eV) scattering from condensed thymine
J. Chem. Phys. **122**, 224704 (2005); 10.1063/1.1925610

The triplet state of cytosine and its derivatives: Electron impact and quantum chemical study
J. Chem. Phys. **121**, 11668 (2004); 10.1063/1.1812533

Measurement of absolute differential cross sections for the excitation of the π,π * triplet state of ethene by electron impact at 0° and 180°
J. Chem. Phys. **106**, 7044 (1997); 10.1063/1.473727

Absolute cross sections for electronic excitation of pyrimidine by electron impact

Khrystyna Regeta,[1] Michael Allan,[1] Zdeněk Mašín,[2] and Jimena D. Gorfinkiel[3]

[1]*Department of Chemistry, University of Fribourg, Chemin du Musée 9, CH-1700 Fribourg, Switzerland*
[2]*Max-Born Institute for Nonlinear Optics and Short Pulse Spectroscopy, Max-Born-Straße 2A,*
12489 Berlin, Germany
[3]*Department of Physical Sciences, The Open University, Walton Hall, Milton Keynes MK7 6AA,*
United Kingdom

We measured differential cross sections for electron-impact electronic excitation of pyrimidine, both as a function of electron energy up to 18 eV, and of scattering angle up to 180°. The emphasis of the present work is on recording detailed excitation functions revealing resonances in the excitation process. The differential cross sections were summed to obtain integral cross sections. These are compared to results of R-matrix calculations, which successfully reproduce both the magnitude of the cross section and the major resonant features. Comparison of the experiment to the calculated contributions of different symmetries to the integral cross section permitted assignment of several features to specific core-excited resonances. Comparison of the resonant structure of pyrimidine with that of benzene revealed pronounced similarities and thus a dominant role of π–π^* excited states and resonances. Electron energy loss spectra were measured as a preparation for the cross section measurements and vibrational structure was observed for some of the triplet states. A detailed analysis of the electronic excited states of pyrimidine is also presented. © *2016 AIP Publishing LLC.* [http://dx.doi.org/10.1063/1.4939077]

I. INTRODUCTION

Pyrimidine (1,3-diazine, see Fig. 1) is a prototype aromatic heterocyclic compound. It serves as a simple model compound for the nucleobases cytosine, thymine, and uracil, making electron collisions with pyrimidine relevant for radiation damage to living tissue and thus for cancer radiotherapy.[1] Electronic excitation plays a key role because it is likely to be the initial step in the process of neutral dissociation.

Pyrimidine is a planar molecule, belongs to the C_{2v} symmetry group, is isoelectronic with benzene, and has a substantial dipole moment of 2.3 D.[2] The presence of two nitrogen atoms in the ring leads to a number of low-lying n,π^* transitions not present in benzene.

A substantial amount of work relevant to the present study has been published. Excited states of pyrimidine were characterized by vacuum ultraviolet (VUV) and electron energy loss (EEL) spectroscopies, and theoretically. Innes *et al.*[3] published a review covering the knowledge up to 1988. Pisanias *et al.*[4] measured an early threshold electron energy loss spectrum revealing excited states at low resolution. Ferreira da Silva *et al.*[5] presented a very extensive study of the excited states of pyrimidine by VUV photoabsorption with a detailed analysis of vibrational structure. They also presented an EEL spectrum in the 2-15 eV energy range, with an incident electron energy of $E_i = 200$ eV and scattering angle $\theta = 10°$, and angular distribution of the absolute cross section for exciting the most intense band at 7.6 eV (10°–100°, $E_i = 100$ eV). Linert and Zubek recently presented a detailed EEL spectroscopy study, including spectra measured at 180°

using the magnetic angle changer, and accompanied by a fit to Gaussian band shapes.[6]

Stener *et al.*[7] reported VUV photoabsorption spectra with careful vibrational analysis and time-dependent density functional (TD-DFT) calculations. Fischer *et al.*[8] reported extensive calculations using several high level models, indicating also the reorganization energies λ_E. They pointed out the importance of vibronic coupling and showed how it causes a double minimum on the lowest triplet potential surface.

Shape resonances in pyrimidine were studied by electron transmission spectroscopy (ETS) by Nenner and Schulz[9] who reported three shape resonances at 0.25 eV ($\tilde{X}\,^2A_2$), 0.77 eV ($\tilde{A}\,^2B_1$), and 4.24 eV ($\tilde{B}\,^2B_1$). They proposed that the last of these three can mix with core-excited resonances of the same symmetry. ETS spectra of pyrimidine were also reported by Modelli *et al.*[10] who identified a core-excited resonance at 5.5 eV.

Jones *et al.*[11] reported absolute experimental differential cross sections (DCSs) for elastic scattering and excitation of the most intense electronic bands of pyrimidine and benzene in the angular range of 15°–90° and incident electron energies of 15 and 30 eV. This work was substantially extended by Jones *et al.*[12] who reported a comprehensive study of differential cross sections (angular distributions in the 10°–90° range) at incident electron energies of 15, 20, 30, and 50 eV. Mašín *et al.*[13] performed experimental, in the 15-50 eV impact energy range, and R-matrix theoretical studies, up to 15 eV, of inelastic electron scattering from pyrimidine. Mašín and Gorfinkiel then presented a comprehensive *ab initio* theoretical
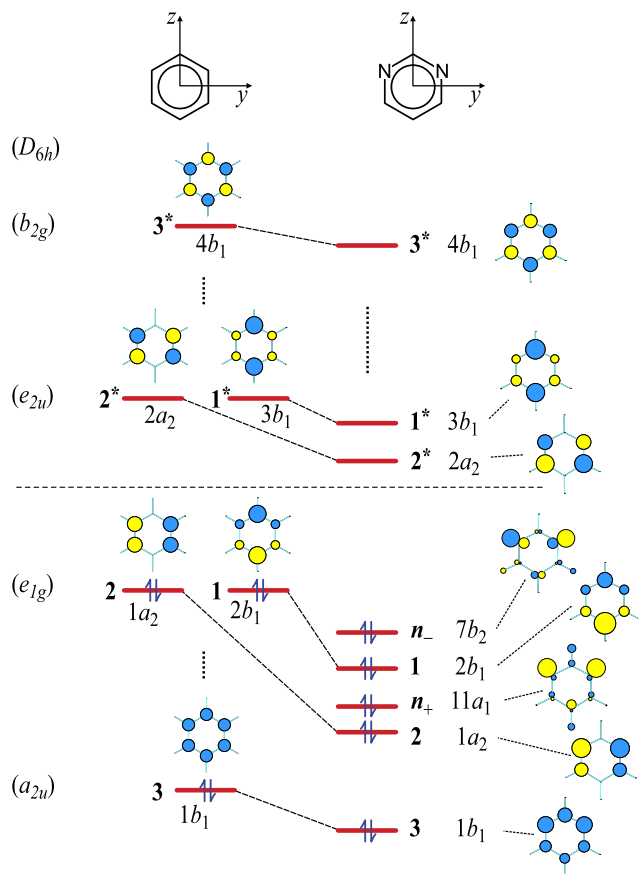
FIG. 1. Qualitative scheme of molecular orbitals involved in the low-lying excited states and the negative ion resonances of pyrimidine (right), compared to those of benzene (left). The relative energies of these orbitals and their occupation in the ground state configurations are also indicated. See text for details of the orbital labeling.

information on resonances is helpful for understanding the excitation mechanism at low energies. The present work thus follows the concept of our recent work on furan.[17] In that case, it was helpful to compare furan (a diene) to the simpler prototype compound ethene. In the same spirit, we compare the pyrimidine spectra and excitation functions to those of the related but simpler molecule benzene.

A series of thorough experimental and theoretical studies were conducted very recently on the somewhat related molecule of phenol.[18–22] They include the study of the excited states[18] but not an analysis of core-excited resonances. The comparison of our results and those for phenol would provide relevant insight into the effect of molecular substitution on scattering but has not been included in this paper for reasons of length.

Data in numerical form are given in the supplementary material.[23]

II. ELECTRON IMPACT SPECTROMETER

The spectrometers and the procedures used to measure the absolute cross sections are the same as in our recent work on furan.[17] The measurements were performed using an electron-impact spectrometer described earlier.[24,25] It employs hemispherical analyzers to improve resolution, which was reduced to 24 meV (in the energy-loss mode) for the present study to gain signal for the weak electronic excitation. The electron beam current was 300-700 pA. The energy of the incident electrons was calibrated on the 19.365 eV ^{2}S resonance in helium[26] and is accurate to within ±10 meV. The sensitivity of the instrument is not constant when the electron energies are varied, and this effect, expressed as the "instrumental response function," was quantified on elastic scattering in helium and all spectra were corrected as described earlier.[24,25] The values of the elastic cross sections were determined by the relative flow technique as described by Nickel *et al.*[27] using the theoretical helium elastic cross sections of Nesbet[28] as a reference and were presented in our accompanying paper.[29] The inelastic cross sections were then determined by comparing the areas under the elastic peak and under the electronic excitation bands of interest as described, for example, in the paper on furan.[17] The technicalities of "tuning" the instrument and of determining the response functions have been described in detail in the work on ethene,[24] CO,[25] and particularly on N_2.[30] The confidence limit is ±15% for the elastic[29] and ±25% for the inelastic cross sections. The pyrimidine and helium pressures in the gas inlet line were typically 0.08 and 0.24 mbar, respectively, during the absolute measurements.

III. R-MATRIX CALCULATIONS

A detailed description of the R-matrix method and its application to electron-molecule scattering can be found elsewhere[31,32] so we will not repeat it here.

The calculations in this work were performed using the same parameters as those reported in earlier papers:[13,14] we used the cc-pVDZ basis set and performed

study of the resonances in pyrimidine (and also in pyrazine and pyridazine), using the R-matrix method and the time-delay analysis, emphasizing core-excited resonances relevant for the present study.[14]

Levesque *et al.*[15] measured vibrational and electronic EEL spectra of pyrimidine condensed on a thin film of solid argon and determined the absolute cross sections for electronic excitation. This work was extended by Michaud *et al.*[16] who presented EEL spectra and absolute cross sections for the electronic excitation of 3 layers of pyrimidine and the DNA bases thymine, adenine, and cytosine by electron impact below 18 eV for molecules deposited at about monolayer coverage on a solid Ar substrate.

The present work aims at expanding the existing experimental studies on electronic excitation by electron impact by extending the energy range to close to threshold, by extending the angular range to 180°, and by providing detailed excitation functions in the near threshold region where they show resonant structure. On the theoretical side, the present work aims at a more detailed presentation of R-matrix calculations, resolved with respect to the electronic states excited and with respect to the symmetry contributions to the integral cross sections, with the goal of, on the one side, a detailed test of theory and on the other side of a theoretical guidance to the assignment of the resonant structure. The

a state-averaged complete active space self-consistent field (SA-CASSCF) calculation using MOLPRO[33] to obtain the target orbitals, wavefunctions, and energies of the 29 electronic states included in the close-coupling expansion. We chose the active space (10, 8), comprising the six valence π orbitals and the two lone-pair orbitals located on the nitrogen atoms.

We employed an R-matrix radius of 13 a_0, continuum GTOs with $l \leq 5$ (for details on the continuum basis set and the L^2 functions used, see Ref. [14]), and the UKRmol+ suite, a re-engineered version of the UKRmol codes.[34] Use of the new parallel suite, capable of determining the molecular integrals in quadruple precision, allowed us to use the complete set of molecular continuum functions generated (in practice, this corresponded to using deletion thresholds of 10^{-14} instead of 10^{-7} as in Ref. [14]). This improvement of the continuum description produced only slightly different results to those presented in the previous work confirming the quality of earlier results. No correction for the limited number of partial waves included in the continuum description has been attempted. We note, however, that inclusion of a Born-type correction increased the total inelastic cross section at most by 5% (at 15 eV) in our previous work.[13] Reference [13] also shows the very small effect that including the $l = 5$ partial waves has on the integral inelastic cross section for energies below 15 eV.

IV. MOLECULAR ORBITALS (MOS)

An introductory review of the MOs will facilitate the understanding of the results of this work. The relevant MOs are shown in Fig. 1. To permit a direct comparison of benzene and pyrimidine, the symmetries for benzene are indicated not only in the D_{6h} group but also in C_{2v}. Consistent orientation of the coordinates was chosen for both molecules (it is shown at the top of the figure), even though it leads to an unusual choice for benzene. It follows from the basic MO principles[35] that the larger nuclear charge of the N-atoms lowers all MO energies. In comparison with benzene, the occupied orbitals $1a_2$ and $2b_1$ of pyrimidine are stabilized more than their unoccupied counterparts $2a_2$ and $3b_1$, reflecting the larger coefficients on the N atoms of the former than the latter. Within both the occupied and the unoccupied manifolds, the a_2 orbitals are stabilized more than the b_1 orbitals because of their larger coefficients on the N atoms.

The major change in pyrimidine compared to benzene is the appearance of the two nonbonding orbitals. The out-of-phase combination n_- lies above the in-phase combination n_+, but both are much higher in energy than the corresponding σ_{C-H} orbitals in benzene. The orbital energies in Fig. 1 are qualitative, but guided by the experimental ionization energies (IEs)[36–38] and vertical attachment energies (VAE).[9,10,39,40] The scheme of the comparison with benzene for the occupied orbitals and the related arguments are identical to those given by the pioneering work of Heilbronner and co-workers.[36] Note that the π and n ordering is not that obtained at the SCF level which predicts the n MOs too low. Short labels of the orbitals, following the numbering of Hashimoto *et al.*,[41] are introduced in bold numbers and letters in Fig. 1 to permit compact designations of transitions in the following
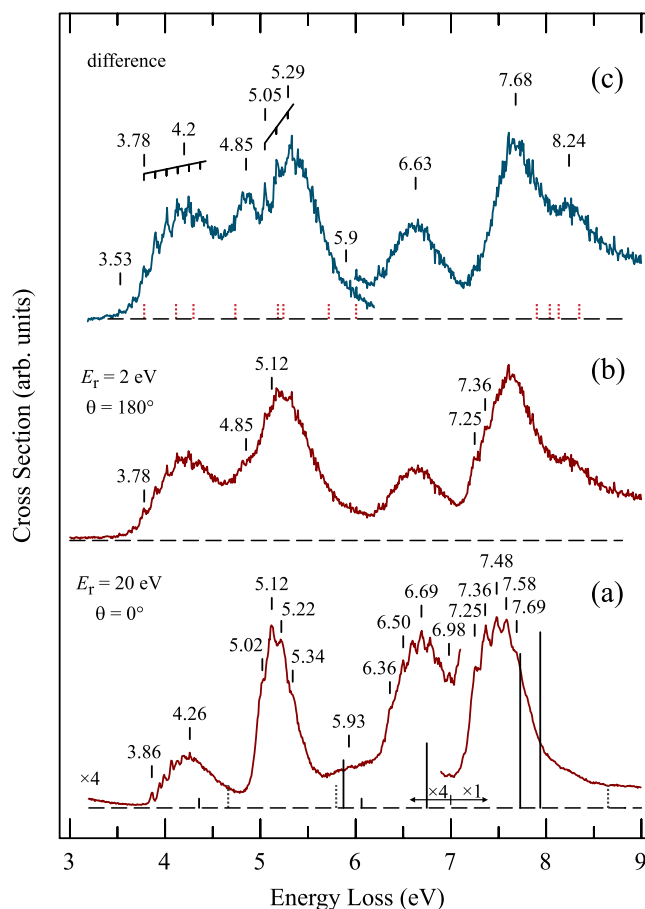

FIG. 2. Representative energy-loss spectra of pyrimidine. The spectrum (a), recorded in the forward direction, shows nearly exclusively dipole allowed transitions. The spectrum (b), recorded in the backward direction with a low residual energy, is dominated by triplet states, but weak excitation of the singlet states can be recognized in some narrow vibronic transitions. The residual contribution of the singlet states has been subtracted from spectrum (b) to obtain the spectrum (c), which shows nearly exclusively triplet states. TD-DFT calculated transition energies are indicated by bars. Triplet states are shown by red dotted bars under the spectrum (c). Singlet states are indicated under the spectrum (a). Allowed transitions are indicated by solid bars with heights indicating the oscillator strength (shown 4× vertically expanded below 7 eV), forbidden transitions by gray dotted bars.

figures, for example, the transition $7b_2 \rightarrow 2a_2$ in pyrimidine is designated as $n_-, 2^*$ in the following.

V. EXCITED STATES OF PYRIMIDINE

We recorded EEL spectra at a number of residual energies and scattering angles as a preparation for measurements of the excitation cross sections and show representative examples in Figs. 2 and 3. Fig. 2 indicates how a difference spectrum showing nearly exclusively triplet states can be constructed and also lists the transition energies. Fig. 3 is devoted to the assignment of the bands and follows the example of Jones *et al.*[11] by comparing the pyrimidine EEL spectra with those of benzene.

Our pyrimidine EEL spectra agree with the published spectra,[5,6,11,12,42] but reveal more vibrational structure in the triplet states which provides useful hints concerning their assignments.
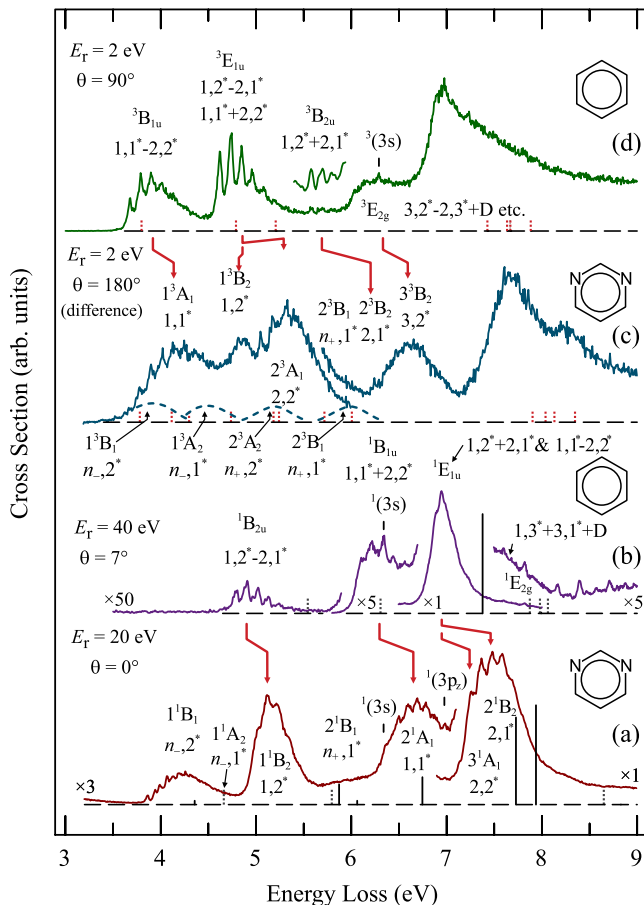
FIG. 3. Comparison of energy-loss spectra of pyrimidine and benzene. Excited states are indicated for both molecules. "D" in the description of the wavefunction indicates a large admixture of doubly excited configurations. Calculated energies are indicated by bars under the spectra as in Fig. 2.

Singlet and triplet excited states have been calculated many times with various models, Refs. 7, 8, and 13 being representative and particularly comprehensive examples. For consistency, and because we needed the oscillator strengths, we show the results of our own TD-DFT calculation with the B3LYP functional and 6-31G* basis set in Figs. 2 and 3, but we also discuss the comparison with the more elaborate published results in the text. Note that the numbering of the totally symmetric states is not consistent in the literature, the first *excited* totally symmetric state being labeled $1\,^1A_1$ in some cases[7] and $2\,^1A_1$ in others[8] ($1\,^1A_1$ being the electronic ground state). We use the latter convention in Fig. 3.

A. Singlet excited states

The bottom spectrum in Fig. 2 was recorded in the forward direction and with a relatively large electron energy, conditions where dipole allowed singlet-singlet transitions dominate. There is general agreement that the first singlet band of pyrimidine is due to the $n_-, 2^*$ (n, π^*) $1\,^1B_1$ transition. Our 0_0^0 energy of 3.86 eV (Fig. 2) agrees with the UV absorption value of 3.854 eV.[5,43] The vibrational structure of the UV band has been analyzed by Ferreira da Silva *et al.*[5] They found that the dominant vibrations are ν_{6a}, ν_{6b}, and ν_{9a}. The ring breathing vibration ν_1 is present but is not

dominant. The fact that several vibrations are active with comparable intensity distinguishes this band from the (π, π^*) bands discussed below.

The next state, a $n_-, 1^*$ $1\,^1A_2$ has a zero oscillator strength (the calculated energy is indicated by a dashed bar under the bottom spectra in Figs. 2 and 3) and we consequently do not see any clear evidence of it in the EEL spectrum. It has been reported in UV absorption[3] and placed at 4.69 eV by Linert and Zubek.[6]

The lowest benzene singlet state $^1B_{2u}$ (see spectrum (b) in Fig. 3) contains two dominant excitations, $1 \to 2^*$ and $2 \to 1^*$ (see Fig. 1 for labels of orbitals), with coefficients of opposite signs.[41] We express this with the compact label $1, 2^* - 2, 1^*$ in Fig. 3. The transition is dipole forbidden and acquires very weak intensity by intensity borrowing from the $^1E_{1u}$ state through the vibronically active vibrational mode ν_{18} (e_{2g}) (pp. 140 and 555 in Ref. 44). The lower symmetry of pyrimidine as compared to benzene has two consequences: (i) the two excitations $1 \to 2^*$ and $2 \to 1^*$ are no longer degenerate and the lower one, $1 \to 2^*$, dominates in pyrimidine and (ii) the transition acquires some oscillator strength and the band is consequently much stronger in the EEL spectrum of pyrimidine than in the EEL spectrum of benzene. The transition in pyrimidine is at slightly higher energy than in benzene—as all (π, π^*) transitions—due to the greater stabilization of the bonding than the antibonding orbitals (Fig. 1). Our 0_0^0 transition energy in pyrimidine, 5.02 eV, agrees with the UV value of 5.01(6) eV of Ferreira da Silva *et al.*[5] The vibrational structure has been assigned to a progression in the ν_1 ring breathing vibration,[5] just like in its benzene counterpart. Note that this state is calculated about 0.7 eV too high in both benzene and pyrimidine by the TD-DFT method, but methods which include doubly excited configurations like CASPT2 or CASSCF[8] make a correct prediction—pointing out that doubly excited configurations participate strongly in the wavefunction of this state.

Signal is clearly observed in the 5.6-6.3 eV region of the singlet pyrimidine spectrum (panel (a) in Figs. 2 and 3) even though it does not have the shape of a band in the proper sense because of overlap with its neighbors $1\,^1B_2$ and $2\,^1A_1$. This $2\,^1B_1$ $n_+, 1^*$ state, which has no analogy in benzene, has a nonzero oscillator strength. It is known from UV absorption[5] and was placed at 6.02 eV by Linert and Zubek.[6]

The second singlet state of benzene, $^1B_{1u}$, contains two dominant excitations, $1 \to 1^*$ and $2 \to 2^*$. The transition is also dipole forbidden and acquires intensity by intensity borrowing from the $^1E_{1u}$ state. The borrowing is much stronger because of the closer proximity to the allowed $^1E_{1u}$ state. Because of loss of orbital degeneracy, the $1 \to 1^*$ excitation dominates in the corresponding $2\,^1A_1$ state of pyrimidine. (This state is called $1\,^1A_1$ in some publications, for example, in Ref. 6, and $2\,^1A_1$ in others, for example, in Refs. 5 and 8—$1\,^1A_1$ being the ground state.) There is great similarity in the vibrational structure of the $^1B_{1u}$ band of benzene and the $2\,^1A_1$ one of pyrimidine, both are dominated by a ring breathing progression as expected for a π, π^* excited state. Note, however, that all vibrational structures superimposed upon this band in pyrimidine have been proposed to be associated with the $7b_2 \to 3s$ Rydberg excitation in the study

of Stener *et al.*[7] In view of the suggestive similarity of the benzene and pyrimidine bands, it appears likely to us that a large part of the structure is due to a ν_1 progression of the valence 2^1A_1 state, as also assumed by Ferreira *et al.*[5]

The assignments of the $^1(3s)$ $7b_2 \rightarrow 3s(a_1)$ and $^1(p_z)$ $7b_2 \rightarrow 3p(a_1)$ Rydberg states in pyrimidine indicated in Fig. 3 are taken from the work of Stener *et al.*[7] Our values of 6.36 eV and 6.98 eV (Fig. 2) agree well with theirs: 6.339 eV and 6.976 eV. Note that the $^1(3s)$ energy in pyrimidine (6.36 eV) is nearly identical to that in benzene (6.34 eV), reflecting the very similar 0_0^0 ionization energies of 9.331 eV[43] and 9.243 eV,[37] respectively. The *vertical* ionization energy of pyrimidine (9.73 eV[36]) is higher than that of benzene (9.45 eV[37]), justifying the positions of the lines in Fig. 1. Note also that the nature of the orbitals is different, π in benzene and n_- in pyrimidine.

Two excitations each dominate the two degenerate $^1E_{1u}$ states in benzene, namely, $1 \rightarrow 2^* + 2 \rightarrow 1^*$ for one and $1 \rightarrow 1^* - 2 \rightarrow 2^*$ for the other. The degeneracy is lifted in pyrimidine, but the two states 3^1A_1 and 2^1B_2 are close to each other and strongly overlap. The spacing of the vibrational structure of these overlapping bands corresponds to ν_1 as for all π,π^* bands. The relative intensities of the vibrational peaks are peculiar—four peaks have nearly the same intensity, followed by two much weaker shoulders. This is explained by the assumption that the first and the third peaks are the origins of the 3^1A_1 and 2^1B_2 bands, respectively, as indicated by the red arrows in Fig. 3. The splitting of the two states is then 0.23 eV, compatible with the results of some calculations (our TD-DFT 0.21 eV, EOM-CCSD 0.23 eV[8]). This assignment also explains the difference in width between the $^1E_{1u}$ band of benzene and the 7.2-7.9 eV band of pyrimidine.

Finally, the broad shoulder around 7.6 eV in the benzene spectrum has been assigned to the $^1E_{2g}$ state which involves excitations from the lowest π and to the highest π^* orbital.[41] It is relatively low in energy because of substantial admixture of doubly excited configurations.[41] It is difficult to decide whether this band has a counterpart in the pyrimidine EEL spectrum.

B. Triplet excited states

The spectrum (b) in Fig. 2 was recorded in the backward direction with the low residual energy of 2 eV and is consequently dominated by spin-forbidden transitions. It agrees well with the near threshold spectra of Palmer *et al.*,[42] and the recent near-threshold spectra of Linert and Zubek.[6] Good agreement is also found with the EEL spectrum of Jones *et al.*;[11] their spectrum recorded at $E_i = 15$ eV, $\theta = 50°$ is about intermediate between the spectra (a) and (b) in Fig. 2.

Details of the vibrational structure in spectrum (b) in Fig. 2, for example, the 7.25 and 7.36 eV features, reveal that dipole allowed transitions also make a small contribution to it. A small amount of spectrum (a) was therefore subtracted from spectrum (b), with a factor chosen such that the vibrational structure attributable to the singlet states disappeared, to yield a nearly pure triplet spectrum, shown as panel (c) both in Figs. 2 and 3. The four π,π^* configurations already discussed for the singlet benzene states are also found in the triplet

manifold in panel (d) in Fig. 3, except that the order is different. The broad nearly structureless band around 6.2 eV in the benzene triplet spectrum has been assigned as the triplet counterpart of the $^1E_{2g}$ singlet state and its energy is also lowered by substantial admixture of doubly excited configurations.

As was the case for the singlet states, the (π,π^*) triplet states of pyrimidine are closely related to those of benzene. They are all slightly shifted to higher energies and dominate over the (n,π^*) triplet states in the spectrum. The 0_0^0 transition from the lowest triplet state has been observed in phosphorescence in the gas phase at 3.537 eV,[3,45] in agreement with a weak feature at 3.53 eV in the EEL spectrum (c) in Fig. 2.

The vibrational frequencies of the 1^3A_1 and 2^3A_1 states observed in Figs. 2 and 3 are 118 and 120 meV (952 and 968 cm^{-1}), respectively, with a confidence limit of about ±40 meV. This corresponds to the mode ν_1 ($8a_1$) (ring breathing, mostly N–N stretch in pyrimidine), with an experimental frequency of 991 cm^{-1} in the electronic ground state.[3] These two values are identical within experimental error and very similar to the benzene values, 112 and 113 meV in the $^3B_{1u}$ and $^3E_{1u}$ states, respectively (ring breathing mode $2a_{1g}$, 993 cm^{-1} in the electronic ground state).

The pyrimidine frequencies can be compared to those of Fischer *et al.*[8] (listed in their supplementary material) who calculated selected excited state frequencies. The comparison for the 1^3A_1 state is complicated by the complex shape of the potential, with two local minima (α and β), both with boat-distorted (C_s) structures, so that four numbers are quoted. The two numbers quoted within the EOM-CCSD model and C_s structures are 959 cm^{-1} (minimum α) and 865 cm^{-1} (minimum β), where the former number is in good agreement with our observation.

Fischer *et al.*[8] describe a complex issue concerning the 1^3A_1 state which they term "breakdown of the alternate-polyene model." They state that this state has two important determinants at the geometry of the ground state (vertical excitation), namely $(1,1^*)$ (coefficient 0.58 in our TD-DFT calculation) and $(2,2^*)$ (coefficient −0.41 in our TD-DFT calculation) (only the dominant determinant $(1,1^*)$ is mentioned in Fig. 3 to prevent overloading the figure). Two localized wells separated by a transition state result; these wells are named $(\alpha)^3A_1$ and $(\beta)^3A_1$ in their paper, and each corresponds to a single-determinant excitation. This has repercussion on the calculation of reorganization energies by an essentially single-reference method (CCSD) which typically overestimates the energies of two-determinant states such as 1^3A_1 at the ground-state geometry. With all this complexity of the potential surface it appears surprising that the 1^3A_1 band in Fig. 3 is dominated by a single progression in the ν_1 mode. The reason could be that the Franck-Condon factors populate primarily the ν_1 states of the (α) structure. A band envelope simulation would be required to solve this issue. (Although $(\beta)^3A_1$ has a mode with imaginary frequency which leads to $(\alpha)^3A_1$ without a barrier. Moreover, $(\beta)^3A_1$ leads directly to $^3B_1$.)

The differences between the vertical and adiabatic energies were determined from the spectra in Fig. 2 and

TABLE I. Comparison of the experimental differences $\Delta\Delta E_{va}$ between the vertical (ΔE_v) and adiabatic (ΔE_a) transition energies with the calculated reorganization energies λ_E (eV).[8]

	ΔE_v	ΔE_a	$\Delta\Delta E_{va}$	λ_E[8]
$1\,^1B_1$	4.26	3.86	0.40	0.46
$1\,^1B_2$	5.15	5.02	0.13	0.19
$2\,^1A_1$	6.69	6.40	0.29	0.42
$3\,^1A_1$	7.48	7.25	0.23	0.28
$(\alpha)1\,^3A_1$	4.20	3.78	0.42	0.46
$1\,^3B_2$	4.85	4.71	0.14	0.20
$1\,^3B_2$	5.29	5.05	0.24	0.18

are compared to the reorganization energies λ_E calculated by Fischer *et al.*[8] in Table I. The vertical transition energies were taken as the band maxima, the adiabatic energies either as the lowest vibrational 0_0^0 in bands with visible vibrational structure or as the estimated band onset otherwise. There is good qualitative agreement between theory and experiment: theory predicts correctly which band will be broad and which narrow, and this agreement provides support for the assignment.

VI. CROSS SECTIONS FOR ELECTRONIC EXCITATION

A. Dependence on electron energy

As in our previous work[17] on furan, the cross sections for electronic excitation were recorded in two steps. First, energy-loss spectra were recorded at the constant incident electron energies E_i of 5, 5.6, 7.6, 10, 15, and 20 eV; they were corrected for the analyzer response function, and the area under the elastic peak was normalized to the elastic cross section reported in our accompanying paper.[29] The integration was done in the energy-loss range from -0.035 eV to $+0.035$ eV, i.e., it excludes vibrational excitation bands. Fig. 4 shows an example of such a constant E_i energy-loss spectrum (except that, for better readability of the figure, the *height* of the elastic peak, not the area under it, was normalized to the absolute cross section). Band overlap prevents measurement of the cross section for individual states and the energy loss range was therefore divided into the 5 ranges I-V as shown in Fig. 4, the dividing lines being at 3.52, 4.78, 5.64, 6.12, 7.02, and 8.16 eV. Integrals of the signal within these ranges yield the desired inelastic differential cross sections.

The energy-loss ranges were chosen in a slightly different way to that of earlier work. Both Michaud *et al.*[16] and Jones *et al.*[12] chose to fit the energy-loss spectra into overlapping Gaussian curves instead of the present non-overlapping ranges. We have chosen this method because Gaussian shapes are often not a good approximation to the Franck-Condon profiles and vibrational structure of our energy-loss spectra and also because of consistency with our earlier work. The disadvantage of our method is, of course, that the cross section of a given segment is "contaminated" by small contribution of states from the neighboring segments. The difference of the two approaches is smaller than it may seem because the tail of the Gaussian which "leaks out" of a given range is largely compensated by the tail of the Gaussian which "leaks in" from
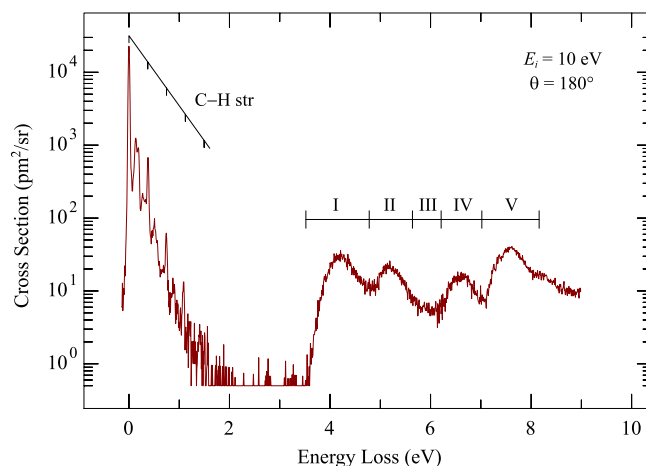

FIG. 4. Representative energy-loss spectrum recorded at a constant incident energy.

the neighboring range. With this in mind the Gaussians I-V of Jones *et al.*[12] correspond nearly exactly to the present ranges I-V and the data may be compared.

The energy-loss spectra also cover the ΔE range with vibrational excitations enabling the determination of vibrational excitation cross sections, all vibrational modes included: the cross sections are discussed in the accompanying paper.[29] Dominant is a long progression of the C–H stretch vibration, which is doubtlessly excited by a very broad σ^* resonance found around 8 eV in all hydrocarbons and generally in all molecules with C–H bonds. This resonance appears in the R-matrix calculations as a very broad feature with a peak at ≈ 11.2 eV in the time-delay spectra and the equivalent resonance has also been observed in calculations for uracil using other methods, see Refs. 46 and 47 and references therein.

In a second step, excitation functions were measured at the energy-losses close to the peaks of the energy-loss spectrum in Fig. 4, at 4.26, 5.20, 5.92, 6.62, and 7.6 eV. The excitation functions, corrected for the analyzer response function, were normalized to the differential cross sections determined by integration under the energy-loss bands as described above. The procedure thus involves an approximation in that the shape of the excitation function reflects the behavior of the peak energy-loss signal, but it is normalized to the area under the energy-loss signal. The discrete absolute values determined from the areas under the energy-loss bands are also shown in the following figures as circles, as a check of consistency.

Note that using excitation functions at a given energy loss (we chose the peak of the band) brings an advantage for comparison of the resonant structure with theory. As a consequence of varying Franck-Condon factors, the position of the resonance peak in the experimental cross section, plotted as a function of energy, shifts when it is measured at different energy losses within a given electronic band (see, for example, benzene, Figures 41 and 42 on p. 272 in Ref. 48). This means that taking the integrals under the energy-loss band will broaden the resonant structure. This broadening is not present in the fixed nuclei calculations, so that the theory-experiment comparison of shapes of the cross sections as a function of
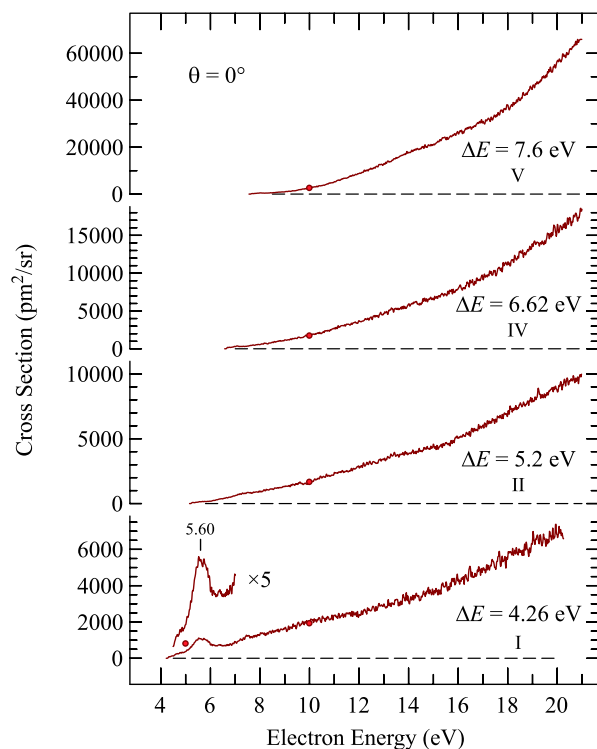
FIG. 5. Cross sections for electronic excitation at 0°. See text for details.
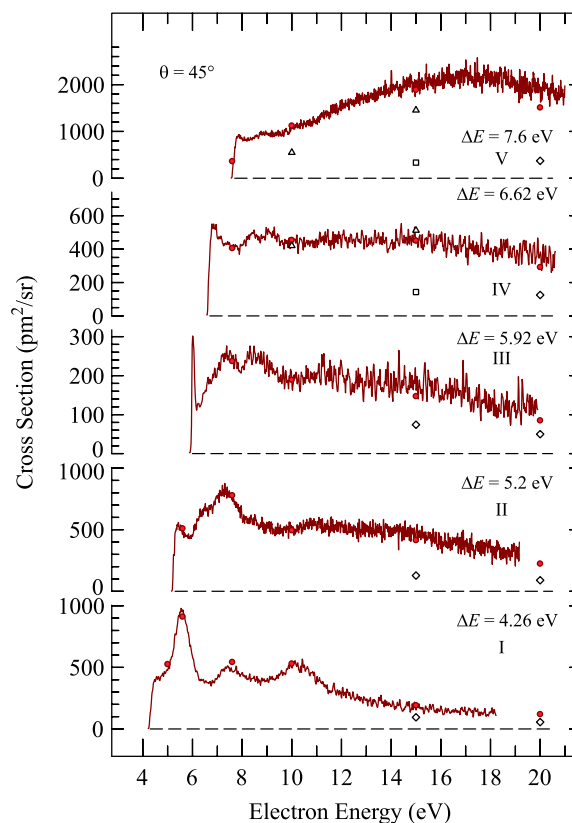

FIG. 7. Cross sections for electronic excitation at 45°. Squares indicate the pyrimidine data of Jones *et al.*,[11] diamonds the pyrimidine data of Jones *et al.*,[12] and triangles the benzene data of Kato *et al.*[49] (Average of the 40° and 50° data is shown in both cases.)

electron energy is more realistic when experimental cross sections measured at a given energy loss are taken.

Elastic cross sections cannot be measured at 0° because the instrument cannot distinguish between elastically forward scattered and unscattered electrons and the inelastic excitation

FIG. 6. Cross sections for electronic excitation at 25°. Diamonds indicate the pyrimidine data of Jones *et al.*,[12] triangles the benzene data of Kato *et al.*[49] (Average of the 20° and 30° data is shown in both cases.)

functions measured at 0° thus cannot be normalized to elastic cross section as described above. The absolute values at 5 and 10 eV were therefore obtained from the angular distributions described in Sec. VI B. The resulting curves are shown in Figs. 5-10.

The cross sections at $\theta = 0°$ in Fig. 5 are dominated by the dipole-allowed states—they rise nearly linearly with energy as expected for a dipole-allowed transitions and attain very high values. There is only one resonant structure, at 5.60 eV in the bottom curve, doubtlessly due to the excitation of the $1\,^3A_1$ state. The linear rise of this curve at higher energies is due to the overlapping $1\,^1B_1$ state, for which the transition is dipole allowed (see Fig. 3).

At higher scattering angles and particularly in the ranges I, II, and III, behavior typical of triplet states is observed—the curves do not rise rapidly and exhibit a number of resonances which will be discussed below.

At the scattering angle of $\theta = 25°$ in Fig. 6 the present data agree very well with the pyrimidine data of Jones *et al.*[12] which is also shown in the figure, except that the present data are slightly larger in the range V. The benzene and pyrimidine data are nearly identical as indicated by the benzene data of Kato *et al.*,[49] also given in Fig. 6. In contrast, the data of Jones *et al.*[11,12] are substantially lower than the present data at the intermediate angles of 45° and 90°, Figs. 7 and 8. The present pyrimidine data are, however, in very good agreement with the benzene data of Kato *et al.*,[49] indicated by triangles in Figs. 7 and 8, especially in the range IV. The present data thus
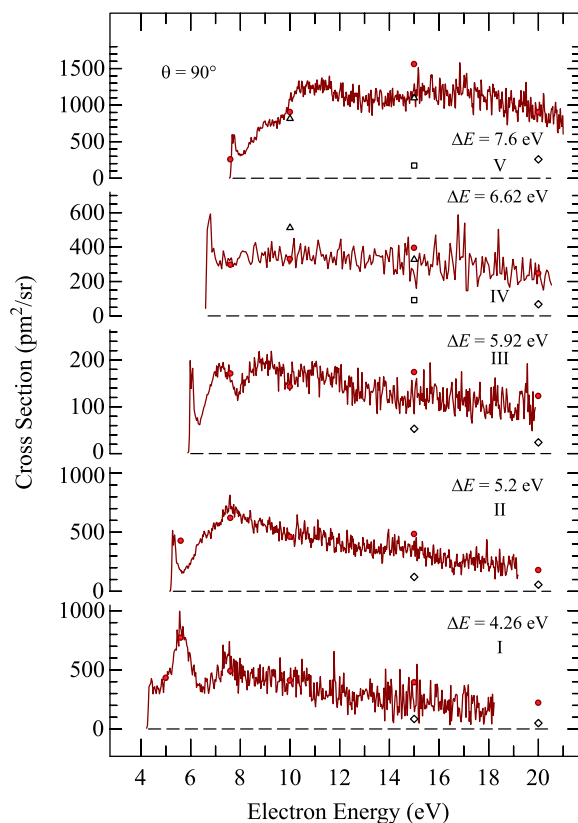
FIG. 8. Cross sections for electronic excitation at 90°. Squares indicate the pyrimidine data of Jones *et al.*,[11] diamonds the pyrimidine data of Jones *et al.*,[12] and triangles the benzene data of Kato *et al.*[49]

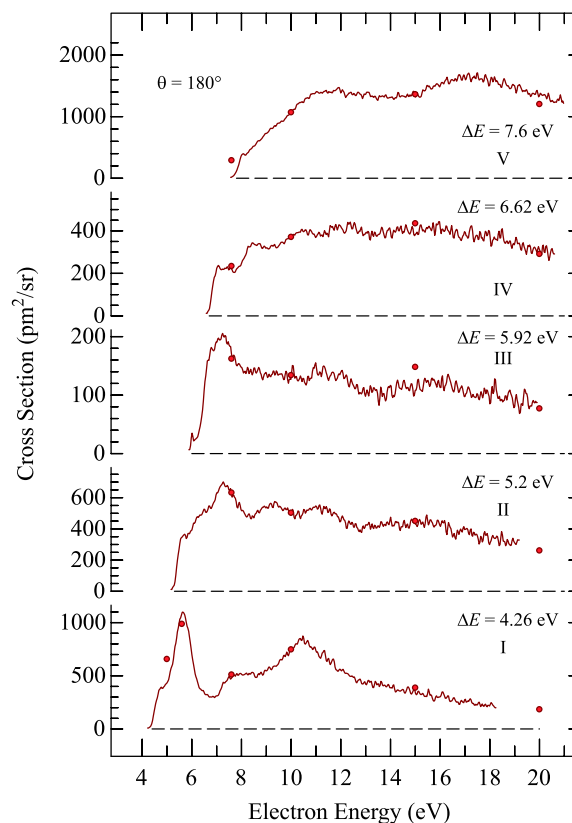FIG. 9. Cross sections for electronic excitation at 135°.

FIG. 10. Cross sections for electronic excitation at 180°.

do not reproduce the difference of the benzene and pyrimidine cross sections at intermediate angles invoked by Jones *et al.*[11]

B. Dependence on scattering angle

To obtain the angular distributions of the inelastic cross sections, electron energy-loss spectra similar to that shown in Fig. 4 were recorded, in a repetitive scan to reduce the effects of drifts, for a large number of angles (with 2.5° increment), controlled by the magnetic angle changer, in ±45° intervals around the mechanically set analyzer positions of 45°, 90°, and 135°. The areas under the electronic energy-loss bands were then evaluated, and the resulting angular distributions were corrected for the angular response functions determined on helium and pieced together to cover the entire 0°–180° angular range. The $v = 0 \rightarrow 1$ vibrational excitation signal in N_2, with a d_π angular distribution, has been used to verify the angular response function in the near-forward direction where helium elastic signal cannot be measured.[30] Finally, the resulting shapes were normalized to the absolute cross section values obtained as described in Section VI A. The results are shown in Fig. 11. The redundancy given by the fact that several absolute points are available for the normalization, at 25°, 45°, 90°, 135°, and 180°, provides a confirmation of the procedure. The individual absolute points are indicated as circles in Fig. 11. Except for the region V, the 10 eV DCSs show increased discrepancy between the absolute point and the relative measurements at 180°, due presumably to a small misalignment of the incident beam and the analyser acceptance cone at 180°. This indicates an increase of our error bar at 180°.
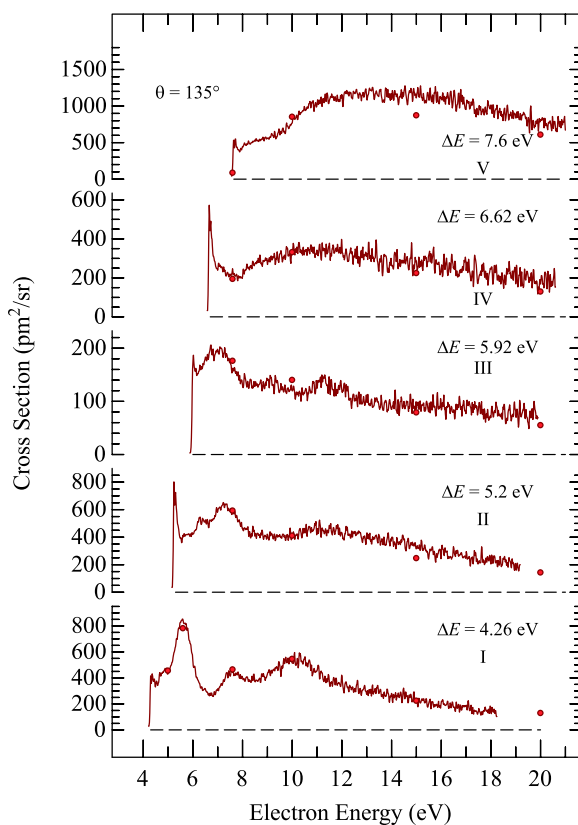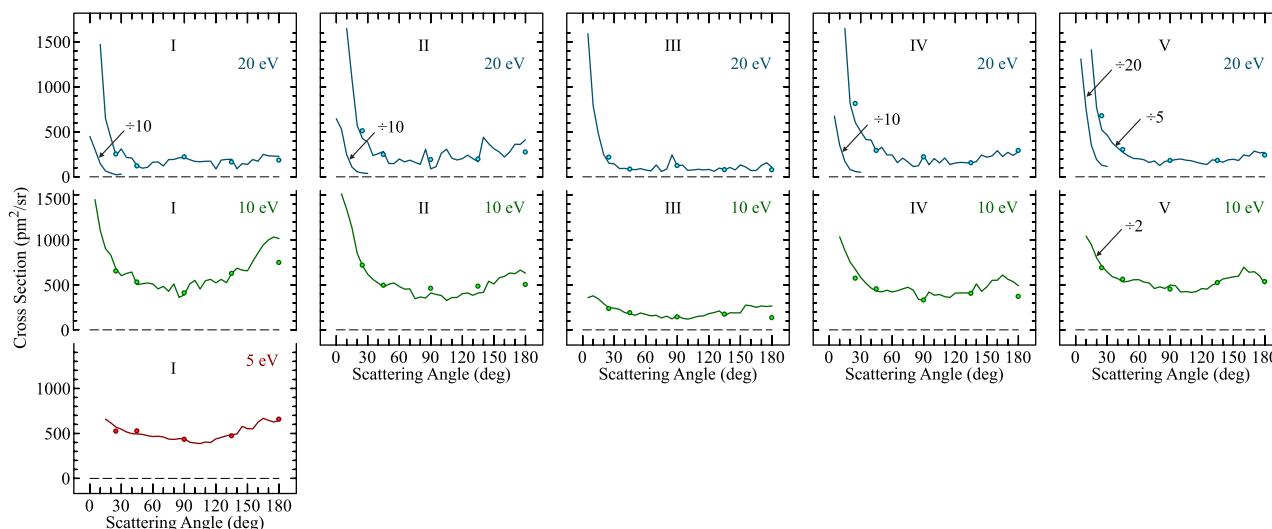
FIG. 11. Angular distributions of electronic excitation. Circles indicate absolute values obtained at 25°, 45°, 90°, 135°, and 180° by comparison with helium. The continuous line was obtained by scanning the magnetic angle changer with increments of 2.5° and normalizing to the values shown by circles. Roman numerals indicate the energy loss ranges (see Fig. 4) over which the cross section was integrated. For easy comparison, the vertical scale is the same for all panels in a given row, except that certain curves or section of curves are shown divided by 2, 5, 10, or 20 as indicated by numbers and arrows.

All cross sections have a narrow peak around 0° at $E_i = 20$ eV due to direct dipole excitation of the dipole-allowed transitions. The cross sections at angles above about 25° are essentially isotropic, characteristic for the excitation of triplet states. The general pattern is thus the same as in the case of furan, except that dipole-allowed transitions are found at all energy losses and they overlap even with the lowest triplet state.

C. Integral cross sections and comparison with theory

Integral cross sections were obtained by numerical integration under the angular distributions of Fig. 11 and

TABLE II. Experimental integral cross sections for electronic excitation, in Å^2. The confidence limit of the present data is ±25%.

	5.0 eV	10 eV	20 eV
This work (range I)	0.598	0.708	0.257
Jones *et al.*[12]	…	…	0.098
Michaud *et al.*[16]	…	0.25	…
This work (range II)	…	0.589	0.352
Jones *et al.*[12]	…	…	0.13
Michaud *et al.*[16]	…	0.35	…
This work (range III)	…	0.225	0.148
Jones *et al.*[12]	…	…	0.061
Michaud *et al.*[16]	…	…	…
This work (range IV)	…	0.555	0.375
Jones *et al.*[12]	…	…	0.154
Michaud *et al.*[16]	…	1.1[a]	…
This work (range V)	…	1.33	1.71
Jones *et al.*[12]	…	…	0.72
Michaud *et al.*[16]	…	0.6[b]	…

[a]Their range III, to be compared with the sum of our ranges III and IV, i.e., with 0.78 Å^2.
[b]Their range IV, at 12 eV.

the results are given in Table II. Comparison with earlier work is complicated by the fact that the energy-loss ranges were chosen in slightly different ways. Both Michaud *et al.*[16] and Jones *et al.*[12] chose to fit the energy-loss spectra into overlapping Gaussian shapes instead of the present nonoverlapping ranges. As already mentioned in Sec. VI A the difference between the two methods is not determining and the Gaussians I-V of Jones *et al.*[12] correspond nearly exactly to the present ranges I-V. Michaud *et al.*[16] measured absolute cross sections in condensed phase, for 3 layers of pyrimidine deposited on a 6-layer spacer of Ar condensed on the Pt substrate. Their Gaussians I, II, and IV correspond well to our ranges I, II, and V; their Gaussian III corresponds approximately to the sum of our ranges III and IV.

The agreement with the data of Michaud *et al.*[16] in Table II is reasonable in view of the very different physical situations in the gas and the condensed phases, and the fact that their value of 1.1 Å^2 for their Gaussian range III, at 10 eV energy, should be compared with the sum of our ranges III and IV, i.e., with the value of 0.78 Å^2. The results of Jones *et al.*[12] are, however, smaller by a factor of more than 2. This cannot be due to different definitions of ranges because the sum of all ranges is also smaller.

The shapes of the experimental differential cross sections as a function of energy from Figs. 5-10 were summed, with appropriate weights, as described in Ref. 25, to obtain the integral cross sections as a function of energy shown in Fig. 12. The result is only approximate in the sense that spectra recorded at only 6 angles were summed. An indication of the magnitude of the error is given by the agreement with the more reliable ICS values from Table II, shown as red circles in Fig. 12, obtained from angular data with a much finer (2.5°) spacing.

Fig. 12 compares the present data to the absolute cross sections of Michaud *et al.*,[16] measured in condensed phase. The agreement is reasonable in view of the fact that the condensed medium is likely to substantially influence the
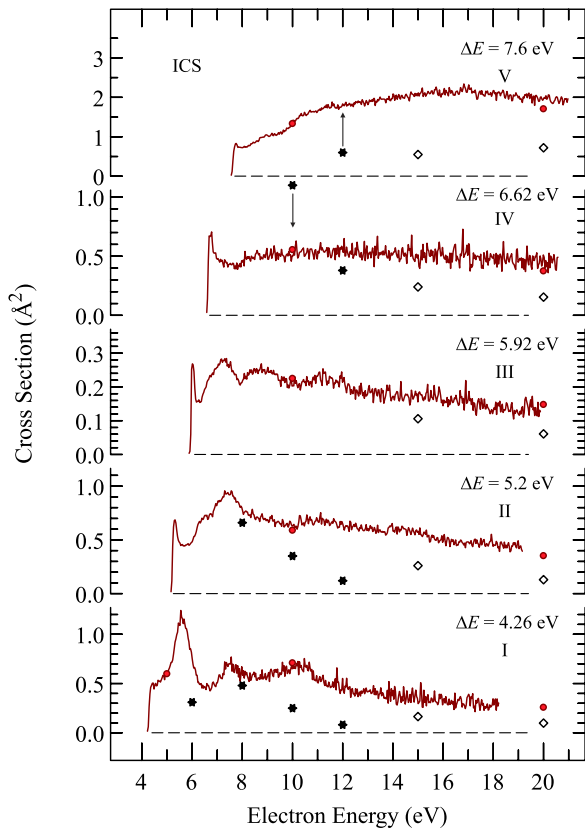
FIG. 12. Integral cross sections for electronic excitation for the energy losses indicated. Circles indicate data obtained by integrating under the angular distributions of Fig. 11 as explained in the text. Diamonds indicate the pyrimidine data of Jones *et al.*,[12] stars the condensed pyrimidine data of Michaud *et al.*,[16] whereby their range IV is compared with our range V, their range III should be compared with the sum of our ranges III and IV, but is compared only with range IV for simplicity.
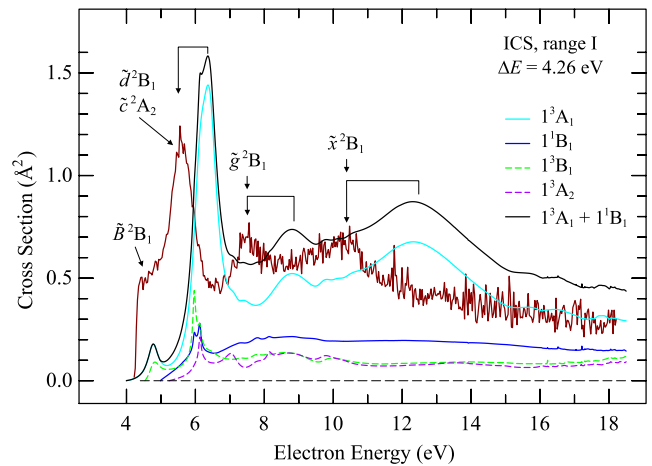

FIG. 13. Integral cross section for electronic excitation of the 4 states lying within range I. The smooth coloured curves are integral cross sections, calculated with the R-matrix method, for exciting the 4 electronic states indicated. The black curve is the sum of the cross sections for exciting the $1\,^3A_1$ and $1\,^1B_1$ states, which contribute to the experimental excitation curve recorded at $\Delta E = 4.26$ eV, shown by the red curve with statistical noise. The $1\,^3B_1$ and $1\,^3A_2$ states are not included in the sum because they lie below/above the energy loss of 4.26 eV (see Fig. 3).

electron-molecule interaction. Fig. 12 further reveals that the ICSs of Jones *et al.*[12] are smaller than the present data. This has already been evident in Table II and on the level of DCSs in Sec. VI A.

The ICS for range I is compared to the theoretical R-matrix results in Figs. 13 and 14. Fig. 13 shows the calculated cross sections for the four states lying within the range I. Reference to Fig. 3 shows that at the energy loss, $\Delta E = 4.26$ eV, at which the excitation function in Fig. 13 was recorded, only two states, $1\,^3A_1$ and $1\,^1B_1$, contribute significantly, and the sum of ICSs for only these two states is shown as a black line in Fig. 13 and should be compared to the experimental red line.

The agreement in the absolute magnitude of the cross section is excellent. There is also very good agreement in the general shape of the cross section, in particular, the existence of a dominant peak which is at 5.55 eV in the experiment and 6.35 eV in the summed (black) curve—that is, theory places the resonance 0.8 eV too high. Other core-excited resonances also appear too high in the R-matrix calculations. Polarization/correlation effects, which play an important role in determining resonance positions and widths, are modeled by including in the close-coupling expansion a number of electronically excited target states coupled to the continuum orbitals and by the L^2 functions.[14] Only a limited number
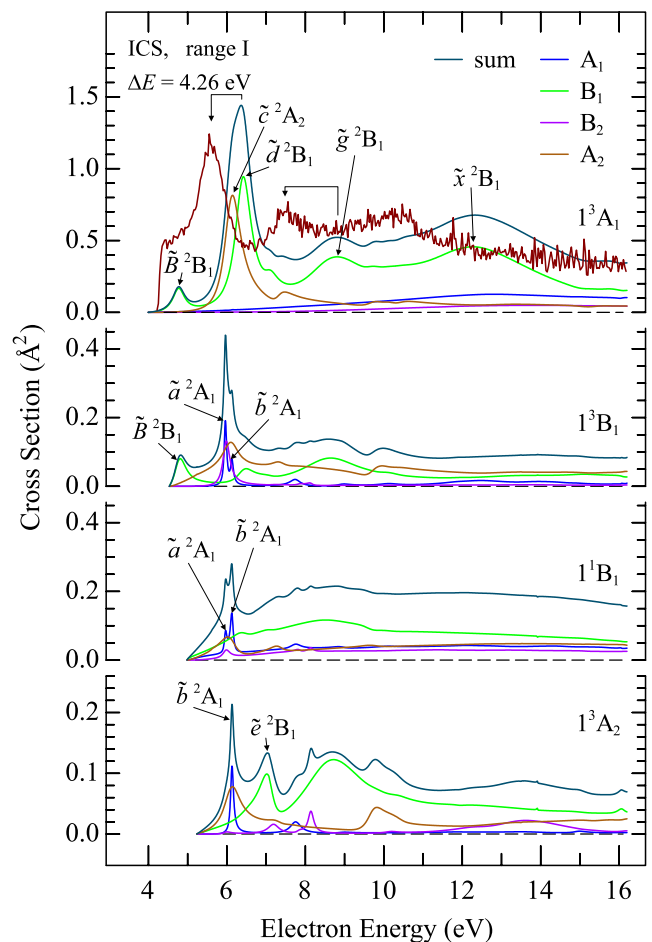

FIG. 14. Contributions of the different symmetries to the excitation cross sections for the four states relevant for range I. For comparison, the experimental data recorded at $\Delta E = 4.26$ eV are shown in the top panel by the red curve with statistical noise.

TABLE III. Vertical excitation energies (in eV) of the states contributing to the EEL in range I calculated by the SA-CASSCF method,[13] used as input to the present R-matrix calculations, and a comparison with the more accurate values of Fischer *et al.*[8]

State	Present theory	Reference 8
1^3A_1	4.00	4.0
1^3B_1	4.54	3.8
1^1B_1	4.99	4.3
1^3A_2	5.24	4.4

of L^2 configurations can be included (given by the size of the Hamiltonian matrix we can routinely diagonalize). In addition, our calculated target electronic states tend to appear higher in energy than more accurate calculations and experiments predict, see Table III. Both facts combine to cause the overestimation of the resonance positions.

There is very good agreement in the first 1.5 eV above threshold where the experiment shows a stepwise onset and a substantial signal, which can be ascribed to the calculated 4.8 eV resonance. The calculated resonance is narrower, but it must be taken into account that the experimental band is broadened by vibrational motion—the Franck-Condon band envelope—absent in the fixed-nuclei calculation. Finally, the shapes of the experimental and theoretical cross sections resemble each other even above 7 eV, with two broad resonances, except that the resonances are calculated too high for the above-mentioned reasons.

We note that selecting the contributing states to the range I using the same criteria as in this work would slightly change the theoretical results in Ref. 13 and improve the comparison with experiment, but the agreement would still be poorer than with the current experimental results. In other words, the improved agreement reported here is not just a consequence of a different choice of integration ranges or contributing states.

The ICS for range II is compared to the theoretical R-matrix results in Figs. 15 and 16. The conclusions are the same as for range I, and the agreement in magnitude is very good and so is the agreement of shapes when the above

FIG. 16. Contributions of the different symmetries to the cross section for exciting the three states relevant for range II. For comparison, the experimental data recorded at $\Delta E = 5.2$ eV are shown in the top panel by the red curve with statistical noise.
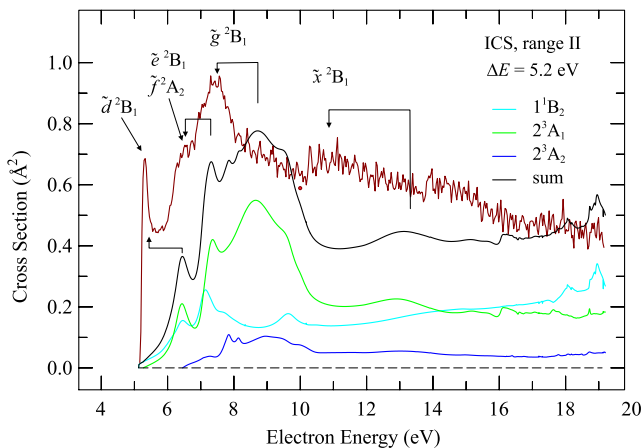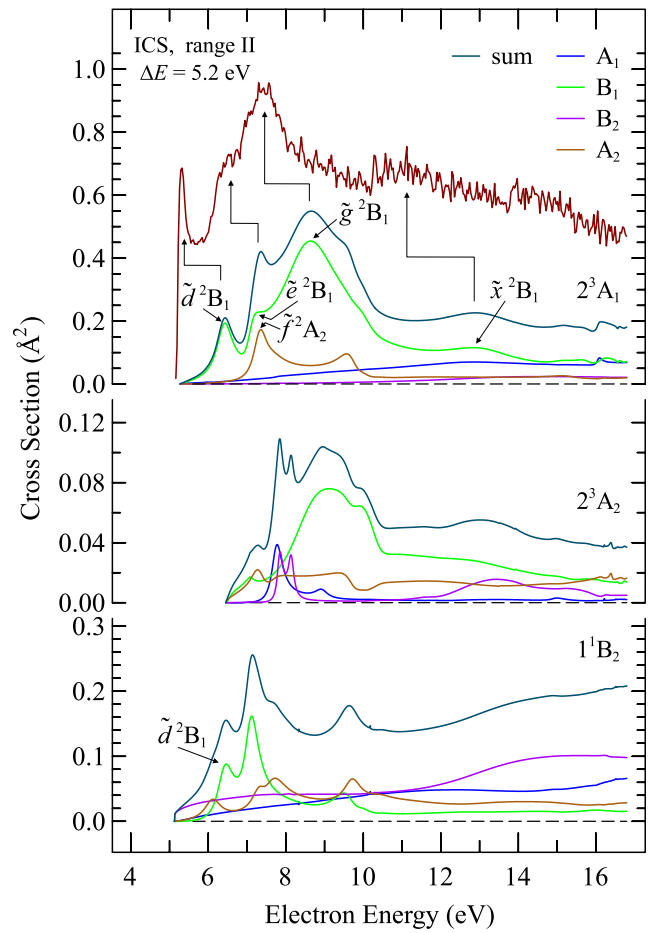

FIG. 15. Integral cross section for electronic excitation of the 3 states lying within range II, indicated on the right. The black curve is the sum of the calculated cross sections for the individual states, the red curve the experimental data.

discussed and well understood tendency of the present method to overestimate resonance energies is taken into account. The calculations include electronically excited states with vertical excitation energies up to 10.51 eV. This cutoff is responsible for the rise of the cross sections above 15 eV and for the unphysical narrow (pseudoresonant) peaks with an onset at ≈ 16 eV.

D. Assignment of resonances

The most important guide to the assignment stems from the comparison of the experiment with the contributions of different symmetries to the calculated cross section, shown in Fig. 14 for range I and in Fig. 16 for range II. The characteristics of the observed and/or calculated resonances are listed in Table IV.

Fig. 13 shows that excitation of the lowest π, π^* excited state 1^3A_1 dominates electronic excitation in range I. The shoulder at threshold is assigned to the $\tilde{B}^2B_1$ resonance, known to be a predominantly shape resonance, making it visible in the elastic cross section[29] and ETS,[9,10] which measures essentially the derivative of the elastic cross section. The fact that it decays into an electronically excited state is taken as a manifestation of an admixture of core-excited configurations

TABLE IV. Selected resonances in pyrimidine. Vertical attachment energies are given. See Refs. 14 and 50 for a more complete list of the calculated resonances.

Label	Expt.	R-matrix	Conf.	ETS[a]	ETS[b]
$\tilde{X}\,^2A_2$	0.27[c]	0.53	2^*	0.25[c]	0.39[c]
$\tilde{A}\,^2B_1$	0.70[d]	0.96	1^*	0.77	0.82
$\tilde{B}\,^2B_1$	4.35	4.78	$3^*+1,2^{*2}+1,1^{*2}$	4.24	4.26
$\tilde{a}\,^2A_1$	…	5.96	$n_-,1^*2^*$	…	…
$\tilde{b}\,^2A_1$	…	6.15	$n_-,1^*2^*$	…	…
$\tilde{c}\,^2A_2$	5.55	6.11	$1,1^*2^*+2,2^{*2}$	…	5.5
$\tilde{d}\,^2B_1$	5.55	6.37	$2,2^*1^*+1,1^{*2}+1,2^{*2}$	…	5.5
$\tilde{e}\,^2B_1$	6.52	7.11	…	…	…
$\tilde{f}\,^2A_2$	6.52	7.33	…	…	…
$\tilde{g}\,^2B_1$	7.45	8.47	…	…	…
$\tilde{x}\,^2B_1$	10.3	12.3	…	…	…

[a]Nenner and Schulz.[9]
[b]Modelli *et al.*[10]
[c]The vibrational origin may lie below 0 eV, making the determination of the vertical attachment energy uncertain.
[d]From the elastic cross section.[29]

in the predominantly shape resonance, as proposed already by Nenner and Schulz[9] and confirmed theoretically by Winstead and McKoy[51] and later on also by the R-matrix calculations.[52] We identified the most important L^2 configurations of the resonances by inspecting the CI coefficients of the R-matrix poles appearing close to the resonance positions as described in Ref. 52. In the present work, the analysis was extended to use the R-matrix poles from the full close-coupling model and not from the simplified close-coupling model of Ref. 52. This analysis identified the leading core-excited configurations $1^*,2^{*2}$, and $1,1^{*2}$ (Table IV) in the nomenclature of Fig. 1. This finding is in agreement with the result of the TD-DFT calculation (see Section VI E) which suggested that the contributing core-excited configuration is $1,1^{*2}$, that is, π,π^{*2}.

Comparison with R-matrix results in Fig. 13 shows that the dominant peak in the experimental spectrum, at 5.5 eV, is mainly caused by the excitation of the lowest π,π^* excited state $1\,^3A_1$. Decomposition of this cross section into contributions from different symmetries, shown in Fig. 14, shows that the peak is due to the two overlapping resonances $\tilde{c}\,^2A_2$ and $\tilde{d}\,^2B_1$. Analysis of the R-matrix basis functions identifies several important configurations based on π,π^* target excitation (see Table IV). These configurations include the $2,2^{*2}$ and $1,2^{*2}$ configurations identified by TD-DFT calculations.

The calculated cross sections for the $1\,^1B_1$, $1\,^3B_1$, and $1\,^3A_2$ states (all three being of the n_-,π^* type) in Fig. 13 indicate a large number of other resonances.[14] Particularly prominent are the two narrow resonances around 6 eV which could be assigned as $\tilde{a}\,^2A_1$ and $\tilde{b}\,^2A_1$ based on the symmetry analysis of Fig. 14. The experimental spectrum does not show evidence of these resonances, presumably because in the experiment the peaks are much smaller and broader due to a broad Franck-Condon envelope. The TD-DFT calculation suggests that the dominant configuration is $n_-,1^*2^*$ in both cases, with the outer shell having once parallel and once antiparallel electrons (Table IV). This result is again in agreement with the analysis of the R-matrix results.

Fig. 13 shows that the two broad structures at 7.45 and 10.3 eV in the experimental spectrum stem primarily from the excitation of the lowest π,π^* excited state $1\,^3A_1$.

Fig. 14 indicates that the resonances are of $^2B_1$ symmetry and they are listed as $\tilde{g}\,^2B_1$ and $\tilde{x}\,^2B_1$ in Table IV. It was not possible to use the analysis of the R-matrix L^2 functions to determine unambiguously the configurations of these two highest-lying broad resonances: their large width prevents us from associating a single dominant R-matrix pole with each of them. However, we note that at energies close to these two resonances configurations of the type $n_-,2^*a_g^*$ start to contribute non-negligibly to the R-matrix basis functions providing tentative evidence that σ^* orbitals are involved in their formation.

We assign the threshold peak in the experimental cross section in the range II (Figs. 15 and 16) to the $\tilde{d}\,^2B_1$ resonance, one of the two resonances responsible for the prominent 5.5 eV peak in the spectrum of range I. The assignment of the higher lying peaks is hampered by the very large number of calculated resonances, seen in the contributions of various symmetries in Fig. 16. We propose that the major contribution to the experimental shoulder at 6.52 eV comes from the $\tilde{e}\,^2B_1$ and $\tilde{f}\,^2A_2$ resonances, and the peak at 7.45 eV is due primarily to the $\tilde{g}\,^2B_1$ resonance.

E. Comparison with benzene

In the remainder of this section, we shall attempt to gain physical insight from comparison of vibrational excitation—indicative primarily of shape resonances—and of electronic excitation—indicative primarily of core-excited resonances—of the two related molecules pyrimidine and benzene. This approach has proven to be insightful for the ethene–furan pair in Ref. 17.

Fig. 17 illustrates the resonant structure of benzene and pyrimidine by representative vibrational and electronic excitation spectra and bears out the great similarity of the resonances of these two isoelectronic molecules. The benzene triplet excitation function is taken from Ref. 53, and the other curves are part of the present work. The benzene triplet excitation function is in agreement with the earlier electron scattering[54] and metastable yield[55] studies. The vibrational excitation spectra confirm the well known π^*
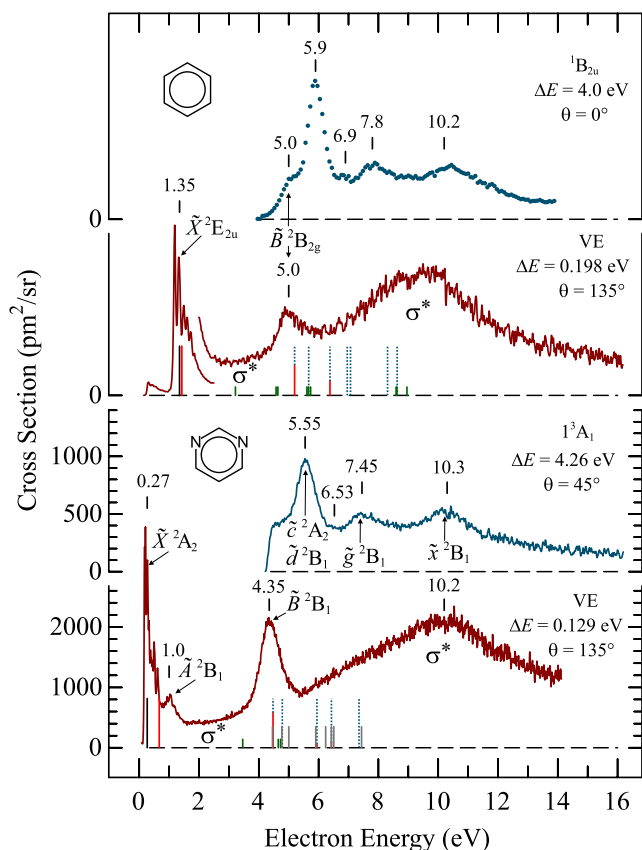
FIG. 17. Excitation functions providing an overview of resonances in benzene and pyrimidine. A representative excitation function for vibrational excitation–providing information primarily on one-particle shape resonances, and a representative excitation function for electronic excitation–providing information primarily on core-excited resonances, are given for each molecule. Vertical sticks indicate results of TD-DFT calculations on the anions, with origins placed at the experimental vertical attachment energies of 0.27 eV for pyrimidine and 1.35 eV for benzene, as indicated by the leftmost (black) stick. Long solid (red) sticks indicate π^* shape resonances, long dotted sticks π,π^{*2} core-excited resonances, short (green) sticks σ^* shape resonances, and intermediate height (gray) sticks n,π^{*2} core-excited resonances. Resonances with significant configuration mixing are indicated by sticks which are in part solid and in part dotted. The benzene spectra are in relative units only.

shape resonances[9,10,39,40] and reveal very broad features with an onset already at the energy of the low-lying π^* resonances and peaking around 10 eV. It is more pronounced in the C–H stretch excitation than in the ring breathing modes and can be assigned to broad overlapping σ^* resonances, of the same nature as recently described in detail theoretically for cyclopropane.[56]

The assignment of the bands in the metastable yield in benzene to core-excited resonances with π,π^{*2} configurations has been forwarded already by Smyth *et al.*[55] As already mentioned above, Nenner and Schulz[9] made the interesting suggestion that the "third" π^* resonance in benzene and pyrimidine may not be pure shape (one particle) resonances but be subject to mixing with close-lying core-excited (two particles one hole) configurations of the same symmetry. The shoulder at 5.0 eV in the cross section for exciting the lowest triplet state in benzene—same energy as the "third" π^* resonance—has been taken as an experimental confirmation of the configuration mixing (CM).[48,53]

It has been shown that qualitative evidence for channel coupling can be obtained from configuration interaction (CI) "electronic structure" calculations on anions although they lack the proper scattering boundary conditions.[51] We used this tool and show the results of TD-DFT calculations in Fig. 17, placing the anion ground states at the lowest experimental vertical attachment energies. The calculations were performed at geometries optimized for the electronic ground states of the neutral targets and reflect thus vertical energies for the attachment of electrons to neutral molecules.

The results are classified by the nature of the orbital occupation in the anionic states: one-particle π^* states (shape resonances) are indicated by solid red vertical bars, π,π^{*2} two particles one hole (core-excited resonances) by cyan dotted bars. Configuration mixing is indicated by bars in part solid red and in part dotted cyan, with the respective heights given by the square of the coefficient of the CI mixing. The concept of resonance parentage foresees that shape resonances decay preferentially to the (vibrationally excited) electronic ground states and are consequently visible primarily in the VE cross sections. The VE spectra in Fig. 17 are thus in good agreement with the calculation—the red bars reproduce well the positions of the 4.35 eV resonance in pyrimidine and the 5.0 eV resonance in benzene. (The observed position of a resonance depends, because of Franck-Condon factors, to some degree on the channel of observation. Thus, the two low-lying shape resonances appear at 0.27 eV and 1.0 eV in the VE spectra in Fig. 17, but were placed at 0.2 eV and 0.70 eV in the elastic scattering study, Table IV and Ref. 29.)

One particle σ^* states (σ^* shape resonances) are indicated by short green vertical bars in Fig. 17. σ^* shape resonances are known to be very broad, strongly coupled to the continuum, and the use of a calculation neglecting this coupling is particularly questionable, but we notice that there is a certain resemblance of the calculated one particle σ^* states (short green sticks) and the very broad background bands in the VE cross sections. The R-matrix calculations provide evidence of only the higher lying σ^* resonances: there is an extremely broad structure of $^2A_1$ symmetry with a maximum at about 11.2 eV in the time-delay, although the shape of this peak is not Lorentzian.[50] No evidence for lower lying σ^* resonances was found in the calculations.

The π,π^* two particle-one hole resonances are expected to decay preferentially to their parent electronically excited states. The 4.35 eV resonance in pyrimidine causes strong signal at the threshold of the excitation of the 1^3A_1 lowest excited triplet states, reflecting the core-excited admixture to the nominally shape resonance as in the benzene case. The TD-DFT calculation further yields the lowest π,π^{*2} pure core-excited states about 0.5 eV above the CM states, fit to explain the prominent peaks at 5.55 eV in pyrimidine and 5.9 eV in benzene in Fig. 17.

The TD-DFT calculation for pyrimidine further yielded a number of n_-,π^{*2} and n_+,π^{*2} core-excited anionic states—they are indicated by the gray (intermediate height) sticks under the lowest spectrum in Fig. 17. They would be expected to decay into the n_-,π^* and n_-,π^* triplet states, but do not make a noticeable contribution to the $\Delta E = 4.26$ eV cross section in Fig. 17, because this curve does not have evident

features which would not be present in benzene. These states correspond to the core-excited resonances (Table IV and Refs. 14 and 50) identified using the R-matrix method. Overall, the experimental results and TD-DFT calculations agree very well with the resonance spectrum determined using the scattering R-matrix method.

VII. CONCLUSIONS

Differential cross sections for electronic excitation were measured for pyrimidine, with emphasis on absolute values and on resonant structures in the energy ranges from threshold to 15 eV. Integral cross sections were obtained by summing the angle-specific data.

The agreement between the experimental and R-matrix integral cross sections for the low-lying electronic states is excellent. Theory not only reproduces the magnitude of cross section accurately, it also reproduces its shape as a function of energy very well, if one accounts for the fact that core-excited resonances are generally calculated higher in energy than observed for the reasons explained in the paper. Given the complexity of performing both measurements and calculations, this agreement is remarkable. The calculated cross sections, separated into contributions of different symmetries, provided insight into the nature of the resonances, particularly the core-excited resonances, and thus into the mechanism of electronic excitation at low energy.

Comparison with the published cross sections for electronic excitation in benzene of Kato *et al.*[49] indicates that cross sections for exciting (π, π^*) states are nearly the same in magnitude for pyrimidine and benzene—as may be expected on the basis of the very similar π orbital structure of the two molecules.

Physical insight and a global overview of resonances has been provided by comparison of selected vibrational and electronic excitation cross sections, and by comparison of pyrimidine and benzene. This comparison reveals great similarity of the resonant processes of the two isoelectronic molecules, although the pyrimidine case is nominally much more complicated because of the high-lying n_- and n_+ orbitals which lead to many (n, π^*) excited states and associated core-excited resonances.

The R-matrix calculations indicate that the cross sections for exciting the (n, π^*) excited states are generally smaller than those for exciting the (π, π^*) states, further enhancing the pyrimidine–benzene similarity. The dynamics of nuclear motion following the excitation is expected to be much more complicated in pyrimidine than in benzene, however, because the (π, π^*) and (n, π^*) excited states are interconnected by vibronic coupling leading to very complex potential surfaces. The (π, π^*) excited states may thus act as doorway states for electron-driven chemical change.

These results, taken together with the results for ethene and furan,[17] indicate that there is a general pattern for electronic excitation of low-lying π, π^* triplet states of molecules with π orbitals, whereby they are excited by higher-lying π^* shape resonances at and immediately above threshold and by π, π^{*2} core-excited shape resonances at higher energies.

Electron energy loss spectra were measured as a preparation for the cross section measurements and two representative spectra were presented. Improved resolution and signal-to-noise ratio permitted us to observe vibrational structure in two triplet states of pyrimidine which provided useful hints concerning their assignment. Physical insight is provided by comparison of well-resolved energy-loss spectra of pyrimidine and benzene. The vibrational structure of the triplet bands further emphasized the great similarity between the electronic structure of the two molecules.

Finally, the R-matrix calculations suggest the presence of a number resonances (some of which are listed in Table IV) that are not visible in the cross sections for pyrimidine prepared in the ground electronic state or are only visible in the inelastic cross sections. These resonances overlap and vibrational motion probably broadens them making them hard to identify in the type of experiments presented here. However, these resonances should appear clearly in experiments which measure the elastic cross section for electron scattering from a low-lying electronically excited state[14,50] and in superelastic experiments, which are more feasible. These types of resonant states may be of relevance for the modeling of atmospheric plasmas where interactions with electronically excited molecules and radicals play an important role. Therefore, their experimental confirmation is highly desirable.

[1]B. Boudaïffa, P. Cloutier, D. Hunting, M. A. Huels, and L. Sanche, Science **287**, 1658 (2000).

[2]G. L. Blackman, R. D. Brown, and F. R. Burden, J. Mol. Spectrosc. **35**, 444 (1970).

[3]K. K. Innes, I. G. Ross, and W. R. Moomaw, J. Mol. Spectrosc. **132**, 492 (1988).

[4]M. N. Pisanias, L. G. Christophorou, J. G. Carter, and D. L. McCorkle, J. Chem. Phys. **58**, 2110 (1973).

[5]F. F. da Silva, D. Almeida, G. Martins, A. R. Milosavljević, B. P. Marinković, S. V. Hoffmann, N. J. Mason, Y. Nunes, G. Garcia, and P. Limão-Vieira, Phys. Chem. Chem. Phys. **12**, 6717 (2010).

[6]I. Linert and M. Zubek, Chem. Phys. Lett. **624**, 1 (2015).

[7]M. Stener, P. Decleva, D. M. P. Holland, and D. A. Shaw, J. Phys. B: At., Mol. Opt. Phys. **44**, 075203 (2011).

[8]G. Fischer, Z.-L. Cai, J. R. Reimers, and P. Wormell, J. Phys. Chem. A **107**, 3093 (2003).

[9]I. Nenner and G. J. Schulz, J. Chem. Phys. **62**, 1747 (1975).

[10]A. Modelli, P. Bolognesi, and L. Avaldi, J. Phys. Chem. A **115**, 10775 (2011).

[11]D. B. Jones, S. M. Bellm, P. Limão-Vieira, and M. J. Brunger, Chem. Phys. Lett. **535**, 30 (2012).

[12]D. B. Jones, S. M. Bellm, F. Blanco, M. Fuss, G. Garcia, P. Limão-Vieira, and M. J. Brunger, J. Chem. Phys. **137**, 074304 (2012).

[13]Z. Mašín, J. D. Gorfinkiel, D. B. Jones, S. M. Bellm, and M. J. Brunger, J. Chem. Phys. **136**, 144310 (2012).

[14]Z. Mašín and J. D. Gorfinkiel, J. Chem. Phys. **137**, 204312 (2012).

[15]P. L. Levesque, M. Michaud, and L. Sanche, J. Chem. Phys. **122**, 094701 (2005).

[16]M. Michaud, M. Bazin, and L. Sanche, Int. J. Radiat. Biol. **88**, 1 (2012).

[17]K. Regeta and M. Allan, Phys. Rev. A **91**, 012707 (2015).

[18]D. B. Jones, G. B. da Silva, R. F. C. Neves, H. V. Duque, L. Chiari, E. M. de Oliveira, M. C. A. Lopes, R. F. da Costa, M. T. d. N. Varella, M. H. F. Bettega, M. A. P. Lima, and M. J. Brunger, J. Chem. Phys. **141**, 074314 (2014).

[19]R. F. da Costa, E. M. de Oliveira, M. H. F. Bettega, M. T. d. N. Varella, D. B. Jones, M. J. Brunger, F. Blanco, R. Colmenares, P. Limo-Vieira, G. Garca, and M. A. P. Lima, J. Chem. Phys. **142**, 104304 (2015).

[20]R. F. C. Neves, D. B. Jones, M. C. A. Lopes, K. L. Nixon, G. B. da Silva, H. V. Duque, E. M. de Oliveira, R. F. da Costa, M. T. d. N. Varella, M. H. F. Bettega, M. A. P. Lima, K. Ratnavelu, G. Garca, and M. J. Brunger, J. Chem. Phys. **142**, 104305 (2015).

[21]R. F. C. Neves, D. B. Jones, M. C. A. Lopes, K. L. Nixon, E. M. de Oliveira, R. F. da Costa, M. T. d. N. Varella, M. H. F. Bettega, M. A. P. Lima, G. B. da Silva, and M. J. Brunger, J. Chem. Phys. **142**, 194302 (2015).

[22]R. F. C. Neves, D. B. Jones, M. C. A. Lopes, F. Blanco, G. Garca, K. Ratnavelu, and M. J. Brunger, J. Chem. Phys. **142**, 194305 (2015).

[23]See supplementary material at http://dx.doi.org/10.1063/1.4939077 for data in numerical form.

[24]M. Allan, C. Winstead, and V. McKoy, Phys. Rev. A **77**, 042715 (2008).

[25]M. Allan, Phys. Rev. A **81**, 042706 (2010).

[26]A. Gopalan, J. Bömmels, S. Götte, A. Landwehr, K. Franz, M. W. Ruf, H. Hotop, and K. Bartschat, Eur. Phys. J. D **22**, 17 (2003).

[27]J. C. Nickel, P. W. Zetner, G. Shen, and S. Trajmar, J. Phys. E: Sci. Instrum. **22**, 730 (1989).

[28]R. K. Nesbet, Phys. Rev. A **20**, 58 (1979).

[29]K. Regeta, M. Allan, C. Winstead, V. McKoy, Z. Mašín, and J. D. Gorfinkiel, J. Chem. Phys. **144**, 024301 (2016).

[30]M. Allan, J. Phys. B: At., Mol. Opt. Phys. **38**, 3655 (2005).

[31]J. Tennyson, Phys. Rep. **491**, 29 (2010).

[32]P. G. Burke, *R-Matrix Theory of Atomic Collisions: Application to Atomic, Molecular and Optical Processes* (Springer, 2011).

[33]H.-J. Werner, P. J. Knowles, R. Lindh, F. R. Manby, M. Schütz *et al.*, MOLPRO, version 2009.1, a package of *ab initio* programs, 2009, see http://www.molpro.net.

[34]J. M. Carr, P. G. Galiatsatos, J. D. Gorfinkiel, A. G. Harvey, M. A. Lysaght, D. Madden, Z. Mašín, M. Plummer, J. Tennyson, and H. N. Varambhia, Eur. Phys. J. D **66**, 58 (2012).

[35]E. Heilbronner and H. Bock, *Das HMO-Modell und seine Anwendung Bd. 1. Grundlagen und Handhabung* (Verlag Chemie GmbH, Weinheim, Bergstr, 1968), Vol. 1.

[36]R. Gleiter, E. Heilbronner, and V. Hornung, Helv. Chim. Acta **55**, 255 (1972).

[37]P. Baltzer, L. Karlsson, B. Wannberg, G. Öhrwall, D. M. P. Holland, M. A. MacDonald, M. A. Hayes, and W. von Niessen, Chem. Phys. **224**, 95 (1997).

[38]D. Holland, A. Potts, L. Karlsson, M. Stener, and P. Decleva, Chem. Phys. **390**, 25 (2011).

[39]L. Sanche and G. J. Schulz, J. Chem. Phys. **58**, 479 (1973).

[40]K. D. Jordan, J. A. Michejda, and P. D. Burrow, J. Am. Chem. Soc. **98**, 7189 (1976).

[41]T. Hashimoto, H. Nakano, and K. Hirao, J. Chem. Phys. **104**, 6244 (1996).

[42]M. H. Palmer, I. C. Walker, M. F. Guest, and A. Hopkirk, Chem. Phys. **147**, 19 (1990).

[43]S. Sato, K. Omiya, and K. Kimura, J. Electron Spectrosc. Relat. Phenom. **97**, 121 (1998).

[44]G. Herzberg, *Molecular Spectra & Molecular Structure III (Polyatomic Molecules)* (Van Nostrand, New York, London, Toronto, 1966), Vol. 3.

[45]T. Takemura, K. Uchida, M. Fujita, Y. Shindo, N. Suzuki, and H. Baba, Chem. Phys. Lett. **73**, 12 (1980).

[46]Y.-F. Wang and S. X. Tian, Phys. Chem. Chem. Phys. **13**, 6169 (2011).

[47]F. A. Gianturco, F. Sebastianelli, R. R. Lucchese, I. Baccarelli, and N. Sanna, J. Chem. Phys. **128**, 174302 (2008).

[48]M. Allan, J. Electron Spectrosc. Relat. Phenom. **48**, 219 (1989).

[49]H. Kato, M. Hoshino, H. Tanaka, P. Limao-Vieira, O. Ingolfsson, L. Campbell, and M. J. Brunger, J. Chem. Phys. **134**, 134308 (2011).

[50]Z. Mašín, "Resonance formation in electron collisions with pyrimidine-like targets," Ph.D. thesis, The Open University, Milton Keynes, UK, 2012.

[51]C. Winstead and V. McKoy, Phys. Rev. Lett. **98**, 113201 (2007).

[52]Z. Mašín and J. D. Gorfinkiel, J. Chem. Phys. **135**, 144308 (2011).

[53]M. Allan, Helv. Chim. Acta **65**, 2008 (1982).

[54]R. Azria and G. J. Schulz, J. Chem. Phys. **62**, 573 (1975).

[55]K. C. Smyth, J. A. Schiavone, and R. S. Freund, J. Chem. Phys. **61**, 1789 (1974).

[56]R. Čurík, P. Čársky, and M. Allan, J. Chem. Phys. **142**, 144312 (2015).